Journal of Materials Chemistry B

ROYAL SOCIETY OF CHEMISTRY

PAPER

View Article Online
View Journal | View Issue

Cite this: J. Mater. Chem. B, 2024, 12, 11817

Electronic interaction-enhanced NO photorelease and photothermal conversion in N-doped carbon dot nanoconjugates

Francesca Laneri,[a] Cristina Parisi,[a] Marta Maria Natile [b] and Salvatore Sortino *[a]

Received 10th June 2024,
Accepted 10th October 2024

DOI: 10.1039/d4tb01264j

rsc.li/materials-b

A nitric oxide (NO) photodonor (**1**) capable of releasing two NO molecules through a stepwise mechanism has been covalently grafted to blue-emitting N-doped carbon dots (**NCDs**). The resulting water-soluble nanoconjugate (**NCDs-1**), *ca.* 10 nm in diameter, exhibits a new absorption band not present in the simple physical mixture of the two components and is attributable to strong electronic interactions between them in the ground state. Blue light excitation of **NCDs-1** leads to NO photogeneration with an efficiency almost one order of magnitude higher than that observed for **1** alone, probably due to a photoinduced electron transfer between the **NCDs** and the grafted **1**. Photoexcitation of the nanoconjugate also results in effective photothermal conversion, which is negligible in the naked **NCDs**. Furthermore, in contrast to **1**, the nanoconjugate liberates NO also under excitation with green light. Finally, the typical blue fluorescence of the **NCDs** is quenched in **NCDs-1** but restored upon the photouncaging of the second NO molecule, providing readable and real-time information about the amount of NO photogenerated.

Introduction

Carbon dots (CDs) are almost spherical carbon nanoparticles with sizes generally less than 10 nm obtained from a variety of readily available carbon precursors.[1] The CD core consists mainly of sp^2 hybrid carbons,[2] while on the surface different organic functional groups, including amine, hydroxyl and carboxylic groups, act as stabilizers and make accessible the surface engineering with additional molecular units.[2–5] CDs show excellent dispersibility, stability, photostability and tunable optical properties.[6–9] These features, combined with the capability to be involved in intra- and intermolecular photoinduced energy and electron transfer processes with suitable functional components,[10–12] render CDs intriguing nanoplatforms for a wide range of applications such as photovoltaics,[13,14] photocatalysis,[15,16] optoelectronics[17,18] and optical sensing.[19,20]

In contrast to traditional quantum dots based on inorganic semiconductors, CDs exhibit much lower toxicity, better biocompatibility, high cell permeability and low production costs.[21] These advantages have made CDs very appealing for several biological applications as suitable nanoscaffolds for drug carriers[22] and as active components for photodynamic and photothermal therapy applications,[23,24] bioimaging,[25] theranostics[26] and phototheranostics.[27]

Nitric oxide (NO), an inorganic free radical with a half-life of *ca.* 1 s in tissues, is a critical bioregulator of vital functions, including vasodilatation, neurotransmission, and hormone secretion in living bodies.[28,29] Besides, it is involved in many biological processes spanning platelet aggregation inhibition,[30] immune response to bacterial, viral, parasite, and fungi infections,[31,32] reduction of radical-mediated oxidation processes,[33] wound healing,[34] and cancer biology.[35] This multifaceted role of NO has opened new and promising scenarios in bio-medicine based on the appropriate use of this free radical as an unconventional therapeutic agent to combat important diseases.[36–39]

Due to its transient nature, the biological effects of NO are strictly dependent on its generation site and can be beneficial or harmful depending on its doses.[40] This spatiotemporal dependence has made the NO precursors activatable by light stimuli, usually named NO photodonors (NOPDs), very appealing given the unique advantage light-triggering offers over other stimuli in controlling the release process in space and time.[41–44] Light is non-invasive, easy to manipulate and ensures the confinement of the site of action of the NOPD at the illuminated area by appropriate positioning of the light beam and the accurate control of the therapeutic doses by tuning the light intensity and the irradiation time.[45]

In recent years, we and others have achieved hybrid nanoconstructs that covalently integrate CDs and NOPDs for potential therapeutic applications.[46–49] These works have proven the persistent emission of the CDs core as a valuable tool

[a] PhotoChemLab, Department of Drug and Health Sciences, University of Catania, Catania, I-95125, Italy. E-mail: ssortino@unict.it
[b] ICMATE-CNR Institute of Condensed Matter Chemistry and Technologies for Energy, National Research Council, Department of Chemical Science, University of Padova, 35131 Padova, Italy

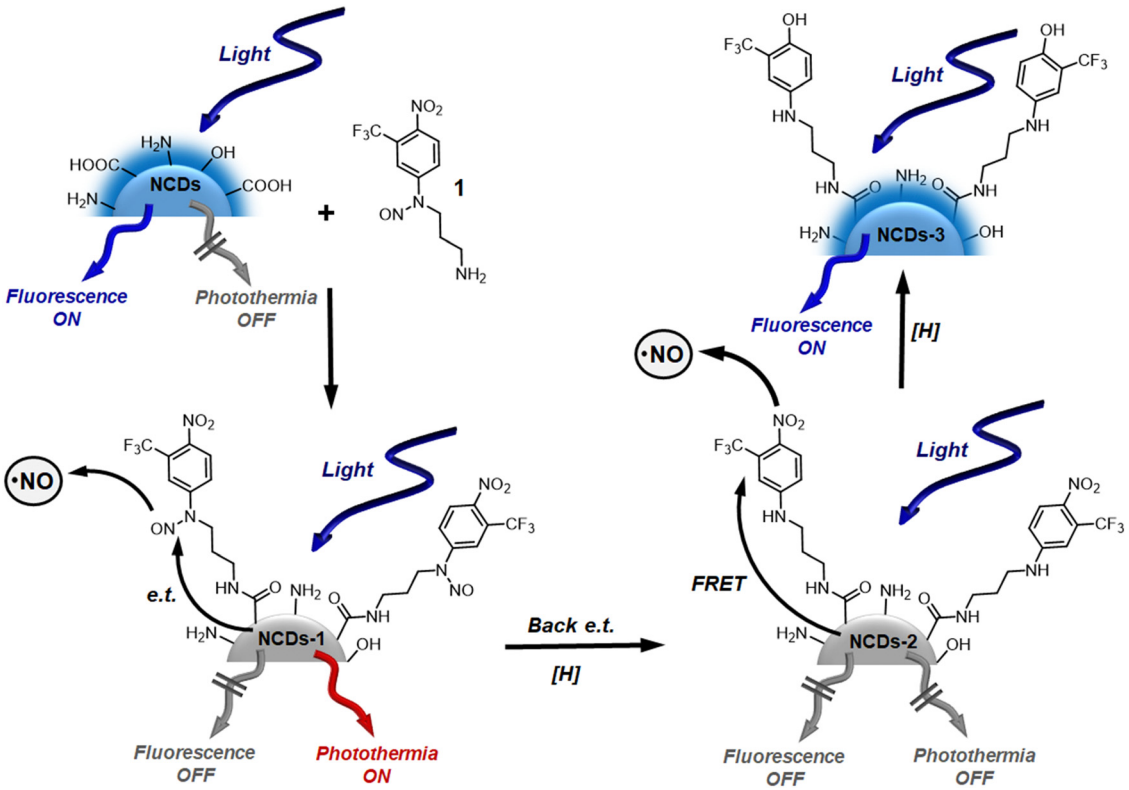

Scheme 1 Sketch of the nanoconjugate **NCDs-1**, formed by condensation of **NCDs** and the NOPD **1**, and its stepwise conversion to **NCDs-2** and then to **NCDs-3** under light excitation.

for tracking the nanoconstruct in a bioenvironment, the activatable emission upon NO photorelease as an intriguing optical reporter to detect NO generation in real time and, finally, the utility of the CDs as two-photon antennae to trigger the release of NO from an otherwise blue-light activatable NOPD exploiting two-photon excitation in the red region.[46–49]

In the frame of our ongoing interest in fabricating multifunctional NO photoreleasing nanoconstructs,[41,50,51] we devised herein the novel CD-based nanoconjugate **NCDs-1** (Scheme 1) and we mainly focus to gain insights into its multifunctional properties. It integrates the NOPD **1**, capable of photorelease two NO molecules under blue light excitation through a stepwise mechanism, into nitrogen-doped CDs (**NCDs**). We show that a core–shell electronic interaction occurring in **NCDs-1** leads to a significant enhancement of efficiency of the first step of NO photorelease if compared with the isolated **1** and, in parallel, to effective photothermal conversion not observed in the naked **NCDs**. Moreover, the typical fluorescence of the **NCDs** core is suppressed in the nanoconjugate but is fully restored concomitantly to the second step of NO photorelease, making the **NCDs** core a fluorescent reporter which provides readable and real-time information about the amount of NO photoreleased.

Results and discussion

Despite its low absorption in the visible region, the NOPD **1** is responsive to 405 nm light stimuli. Excitation of a solution of **1** at this wavelength leads to the absorption spectral changes reported in Fig. 1 typical for biphasic photolysis. The first step (Fig. 1A) is characterized by a bleaching of the main absorption UV band at 290 nm, a new and intense absorption growth with a maximum at 398 nm and the presence of two isosbestic points. Prolonged irradiation with the same excitation source induces bleaching of this new band at 398 nm accompanied by an absorption growth below 300 nm and the appearance of two isosbestic points (Fig. 1B). Fig. 1C reports the absorbance evolution monitored at 398 nm as a function of the irradiation time in which the biphasic photobehaviour can better be noted. Isosbestic points in both the photolysis steps indicate clean photochemical processes. The spectral profiles reported in Fig. 1 are the same as those we have recently observed for **1** in a similar solvent mixture[52] as well as for the hydrophobic analogue of **1** based on the identical chromophoric motif[53] and account well for the release of two NO molecules generated with different rates through the stepwise mechanism illustrated in Fig. 1D.

The first photolytic step involves the homolytic rupture of the N–NO bond, typical for this *N*-nitrosoaniline moieties,[54–56] and the formation of **2** as the only stable photoproduct characterized by the typical absorption band at 398 nm due to the push–pull character of the nitroaniline chromophore.[57–60] The second photolytic step is typically observed for irradiating several derivatives of the 4-nitro-3-(trifluoromethyl)aniline chromophoric scaffold extensively used in our group, leading to phenol derivative **3**, absorbing in the UV region and responsible for the photobleaching observed.[61–64] The quantum yields

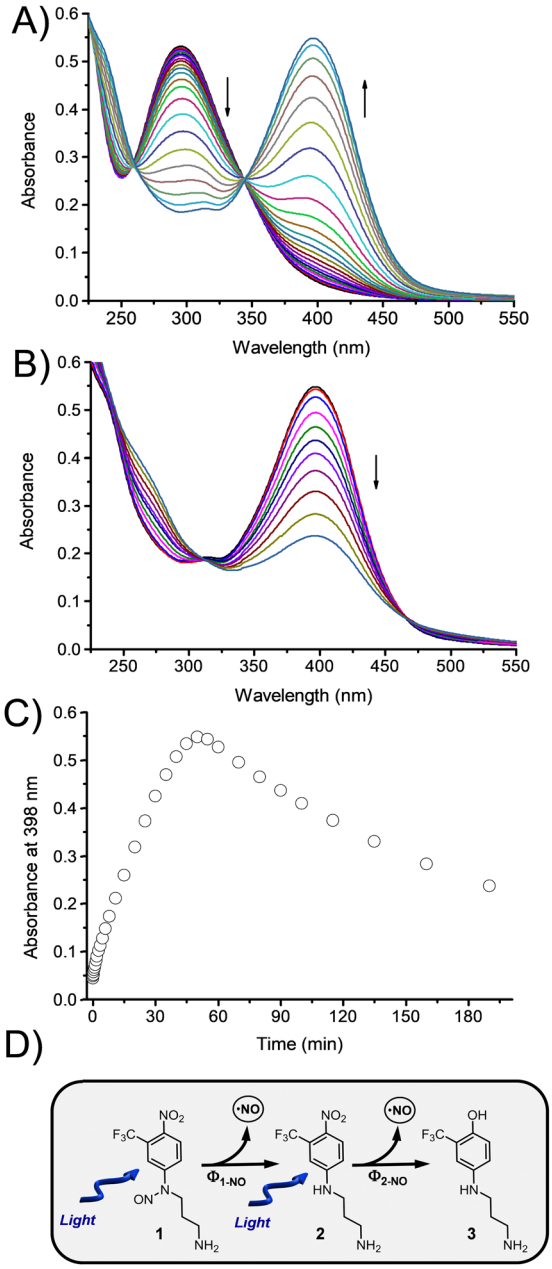

Fig. 1 Absorption spectral changes observed upon exposure of an air-equilibrated aqueous solution of **1** (60 μM) at λ_{exc} = 405 nm at different irradiation times from 0 to 40 min (A) and from 40 to 190 min (B). The arrows indicate the course of the spectral profile with the illumination time. (C) Evolution of the absorbance at 398 nm as a function of the irradiation time. (D) Stepwise mechanism for the NO photorelease and molecular structures of the photoproducts **2** and **3**.

related to the two sequential processes under these experimental conditions were $\Phi_{1\text{-NO}}$ = 0.03 and $\Phi_{2\text{-NO}}$ = 0.7 × 10^{-3}, respectively.

Luminescent **NCDs** were prepared according to the known hydrothermal synthetic protocol based on citric acid and urea as starting materials.[65] These scaffolds are less than 10 nm in diameter and characterized by the presence of –NH_2, –OH and –COOH functional groups, as confirmed by the FTIR analysis

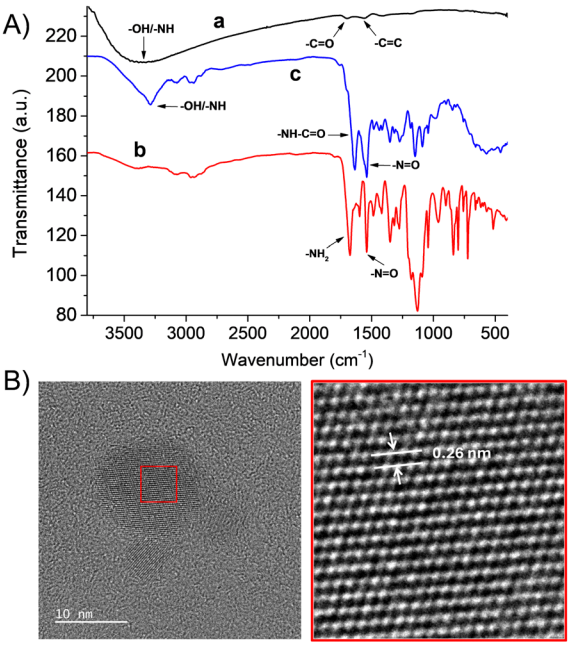

Fig. 2 (A) FTIR spectra of **NCDs** (a), **1** (b) and **NCDs-1** (c). (B) Representative HRTEM images of **NCDs-1**.

(Fig. 2A). The spectrum of **NCDs** shows a broad band from *ca.* 3800 cm^{-1} to 2800 cm^{-1}, ascribed to the stretching frequency of –OH, –NH and COOH groups present on the surface, which make the nanostructure water soluble and suitable for further functionalization. **NCDs-1** were then achieved by condensation of **NCDs** and **1**, purified by dialysis and then freeze-dried (see Experimental section). FTIR analysis demonstrated the successful anchoring of **1** at the **NCDs** surface (Fig. 2A). The stretching vibration at 1560 cm^{-1} belonged to C=C, and the distinctive vibration band at 1700 cm^{-1} was related to the C=O stretching of the carboxylic groups. This peak was shifted to 1635 cm^{-1} in the **NCDs-1** sample, suggesting the formation of an amide bond. The –N=O stretching vibration occurring at 1540 cm^{-1} in free **1** is also evident in the nanoconjugate. HRTEM images (Fig. 2B) show that NCDs are quite spherical with sizes ranging from 5 to 11 nm. The well-resolved lattice fringes with interplanar spacing of 0.26 nm agree with (020) diffraction facets of graphitic carbon.[66]

Analogously to the naked **NCDs**, the nanoconjugate **NCDs-1** was soluble in water with 1% MeOH and remained stable for more than one month under these conditions without any significant signs of aggregation (confirmed by the unaltered UV spectrum).

Fig. 3A shows the absorption spectra of **NCDs-1** and, for comparison, those of the same amounts of the free components **NCDs** and **1**. According to the grafting of **1** on the **NCDs'** surface, **NCDs-1** exhibits the fingerprints of both components as proven by the absorption at *ca.* 330 nm, typical of **NCDs** and at *ca.* 295 nm, typical for **1**. However, the nanoconjugate shows a new absorption band beyond 400 nm and extending up to *ca.* 500 nm. These absorption features differ from the simple superposition of the absorption of the two components since

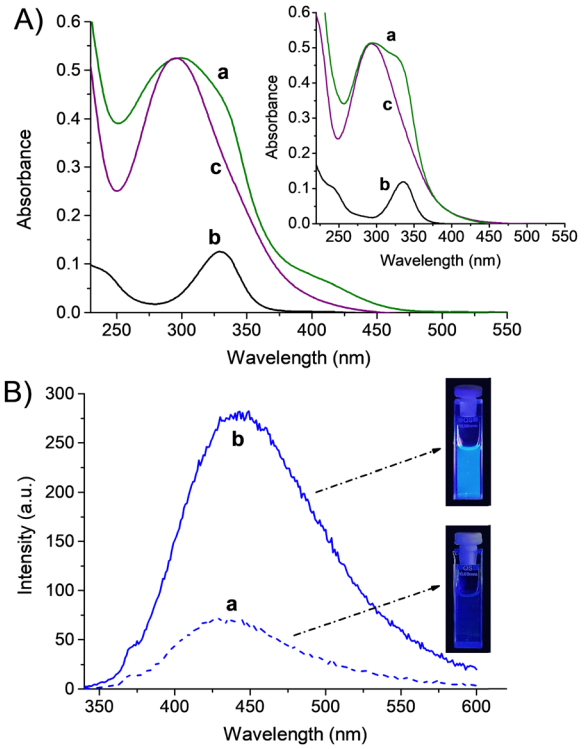

Fig. 3 (A) Absorption spectra of aqueous solutions (1% MeOH) of **NCDs-1** (26 μg mL^{-1}) (a), **NCDs** (b) (10 μg mL^{-1}) and **1** (16 μg mL^{-1}) (c). The inset shows the absorption spectra of the physical mixture of the **NCDs** and **1** at the same concentrations (a) and the isolated components **NCDs** (b) and **1** (c). T = 25 °C. (B) Fluorescence emission spectra (λ = 330 nm) of **NCDs-1** (a) and **NCDs** (b) under the same conditions as in (A). The inset shows the actual images of the samples under UV light illumination (λ_{exc} = 320–360 nm). T = 25 °C.

NCDs do not show any significant absorption beyond 400 nm. Such an absorption cannot be ascribed simply on changes in the molar extinction coefficient of **1** after its grafting on **NCDs** (*vide infra*). Instead, it can result from strong electronic interaction between **NCDs** and **1** in the nanoconjugate in the ground state. This was confirmed by the absence of such a new band in the case of the physical mixture of **NCDs** and **1** under otherwise experimental conditions (inset Fig. 3A). Based on the electron accepting nature of **1** and the electron donating property of **NCDs**, the new band is probably charge transfer in nature. This hypothesis is well supported by a recent study by Guldi and coworkers, who observed the formation of this new absorption band, in their case extending even in the red region, in nanoconjugates of CDs functionalized with strong electron acceptor chromophoric components.[67]

Fluorescence measurements also confirmed electronic interactions in **NCDs-1**. According to the literature, **NCDs** show excellent emission properties with maximum dependence on the excitation wavelength but falling in the blue region in all cases.[65] Fig. 3B shows that the typical emission of **NCDs** observed at λ_{exc} = 330 nm (with fluorescence quantum yield Φ_f = 0.10, see the Experimental section) is quenched in **NCDs-1** (Φ_f = 0.016). Due to the simultaneous absorption of **1** at the excitation wavelength (see Fig. 3A), the emission spectrum of **NCDs-1** has been corrected for the reduced amount of photons absorbed by **NCDs** in the nanoconjugate. Therefore, the fluorescence quenching observed is not due to a trivial effect and demonstrates a strong interaction in the excited state, opening energy and electron transfer quenching mechanisms. We believe that the former is less probable due to the minimal spectral overlap between the emission spectrum of **NCDs** (the potential energy donor) and the absorption spectrum of **1** (the potential energy acceptor). In contrast, according to the literature, a photoinduced electron transfer between the NCDs and **1** seems more likely.[67]

Photolysis experiments were then carried out with a solution of **NCDs-1** under identical experimental conditions to those for free **1**. As shown in Fig. 4A, light irradiation leads to spectral changes similar to those observed for free **1** (see Fig. 1A for the sake of comparison), characterized by the bleaching of the band at *ca.* 300 nm accompanied by the formation of the intense absorption band with the push–pull character at 398 nm. This spectroscopic behaviour aligns with the photorelease of the first molecule of NO from **NCDs-1** (see Fig. 1A) and the formation of **NCDs-2** as a stable photoproduct (see Scheme 1).

Interestingly, as shown in the inset of Fig. 4A, the phototransformation rate of this process was much faster than that observed for **1**. At first sight, this higher conversion rate can be trivially attributed to the higher absorption of **NCDs-1** when compared to **1** at the excitation wavelength (see spectra **a** and **c** in Fig. 3A). However, this is not the case. Even after correction for the different fractions of photons absorbed at 405 nm, the phototransformation of **NCDs-1** was always faster than **1**. Accordingly, photoregulated NO release was confirmed by the typical NO release profile obtained by the direct amperometric detection of this species alternating cycles of light/dark. Fig. 4B clearly shows that NO is released upon illumination, stops in the dark, and restarts once the irradiation source is switched on. The different slopes obtained for **NCDs-1** and, for comparison, free **1** allowed a quantum yield related to the first photolytic process $\Phi_{1\text{-NO}}$ = 0.24 to be obtained, which is *ca.* 8-fold higher than that for the unbound **1**.

From these data, it appears clear that the crucial role of the new charge transfer band of **NCDs-1** is to encourage the NO photodetachment. Based on the already discussed charge transfer character of this band (*vide supra*), we believe a probable explanation for this enhancing effect could involve the radical anion centred on the nitroso group formed after intramolecular electron transfer as the key intermediate. The formation of NO-centred radical anions can be reasonably responsible for releasing NO and, after back electron transfer (back e.t.) and H transfer from the solvent, for the formation of **NCDs-2** (see Scheme 1). This hypothesis is supported by the fact that radical anions of nitroso-derivatives possess a lower dissociation energy of the N–NO bond than their neutral form, encouraging fast NO detachment.[68] Moreover, a similar mechanism was proposed in our recent work in the case of similar nitroso-derivatives photostimulated by appropriate photosensitizers.[69,70]

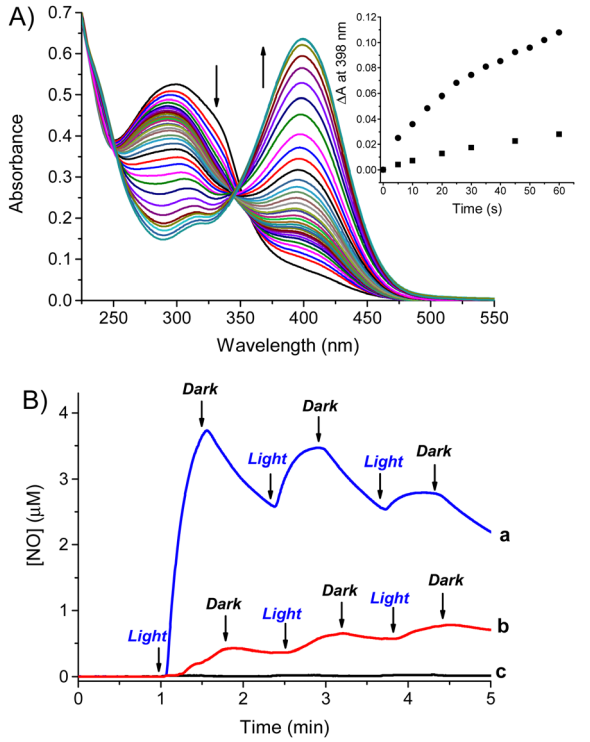

Fig. 4 (A) Absorption spectral changes observed upon exposure of an air-equilibrated aqueous solution (1% MeOH) of **NCDs-1** (26 μg mL^{-1}) at λ_{exc} = 405 nm at different irradiation times from 0 to 39 min. The arrows indicate the course of the spectral profile with the illumination time. The inset shows the difference of absorbance observed at 398 nm for **NCDs-1** (●) and, for comparison, the free **1** (■), in the early stage of the photoreactions. (B) NO release profile observed for an air-equilibrated aqueous solutions (1% MeOH) of **NCDs-1** (26 μg mL^{-1}) (a) and, for comparison, **1** (16 μg mL^{-1}) (b) and **NCDs** (10 μg mL^{-1}) (c), upon alternate cycles of light irradiation at λ_{exc} = 405 nm. T = 25 °C.

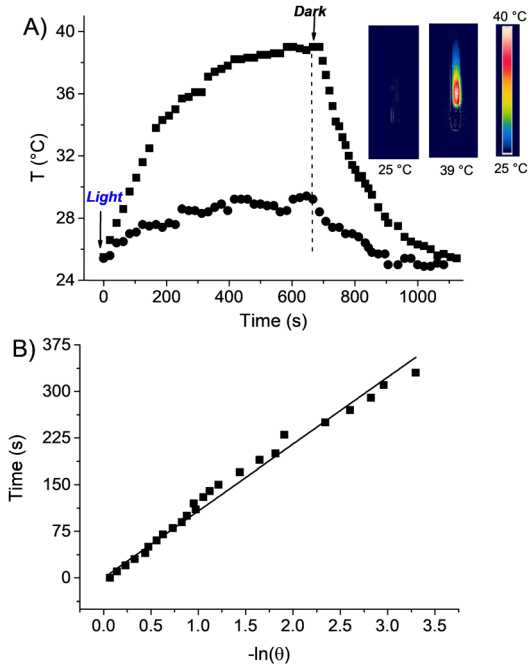

Fig. 5 (A) Temperature changes observed upon 405 nm light excitation of aqueous solutions of **NCDs-1** (26 μg mL^{-1}) (●) and, for comparison, naked **NCDs** (10 μg mL^{-1}) (○). The inset shows representative thermographic images of the **NCDs-1** sample recorded before (left) and after the complete cycle of illumination (right). (B) Linear time data *versus* −ln(θ) obtained from the cooling period of **NCDs-1** in (A).

Note that during the first photolytic step, the emission of **NCDs-1** remains quenched. In this case, the quenching is more likely due to Förster resonance energy transfer (FRET),[71–73] according to the significant spectral overlap between the emission of **NCDs** and the absorption of **2**, as already reported for similar conjugated **NCDs**.[46,47]

The direct participation of the **NCDs** core in the formation of the new charge transfer absorption band of **NCDs-1**, as well as in the mechanism of the NO release enhancement, is confirmed by the photothermal experiments carried out upon 405 nm light excitation (Fig. 5).

Among the variety of properties CDs are also known to possess high photothermal conversion efficiency, with excellent prospects in photothermal therapy applications.[24] In our case, the naked NCDs prepared with the protocol used show a negligible absorption at 405 nm, resulting in a negligible photothermal effect. In contrast, photoexcitation of **NCDs-1** at the same wavelength shows a relevant photothermal action with a temperature raise from *ca.* 25 °C to *ca.* 40 °C in a few minutes (Fig. 5A). The conversion efficiency η (see the Experimental section for the detailed calculations) was ∼40%, a value in excellent agreement with that reported for CDs and other carbon-based photothermal agents.[74] Since, of course, **1** does not show any photothermal action, the photothermia observed confirms well the involvement of the **NCDs'** core in the charge transfer absorption band.

Fig. 6A shows the photolysis of the nanoconjugate for prolonged irradiation times. The spectral changes observed were very similar to those of free **1** (see Fig. 1B for sake of comparison), according to the release of the second molecule of NO and the formation of **NCDs-3** as the stable photoproduct. In contrast to the first photolytic step, no changes in the photolysis rate were observed (see inset of Fig. 6A), suggesting a good retention of the photochemical properties of the NO photoreleaser in the nanoconjugate.

According to the literature, the release of NO from the nitroaniline derivative **NCDs-2** takes place through a nitro-to-nitrite rearrangement[64] in which the **NCD** core is not expected to play any role, in agreement with the similar kinetic behaviour observed. In contrast, the **NCD** core plays a role in the emissive behaviour accompanying the second photolytic step. As shown in Fig. 6B, a significant increase in the fluorescence emission accompanied by a blue shift of the maximum was observed upon irradiation. As already observed for a nanoconjugate similar to **NCDs-2**,[46] the fluorescence increase is due to suppression of the FRET process due to the absorption band's disappearance at 397 nm of the energy acceptor.[46] Interestingly, this fluorescence enhancement makes the **NCD** core an optical counter for the NO.[50] The starting point of the fluorescence restoration represents an indication that the first photolytic

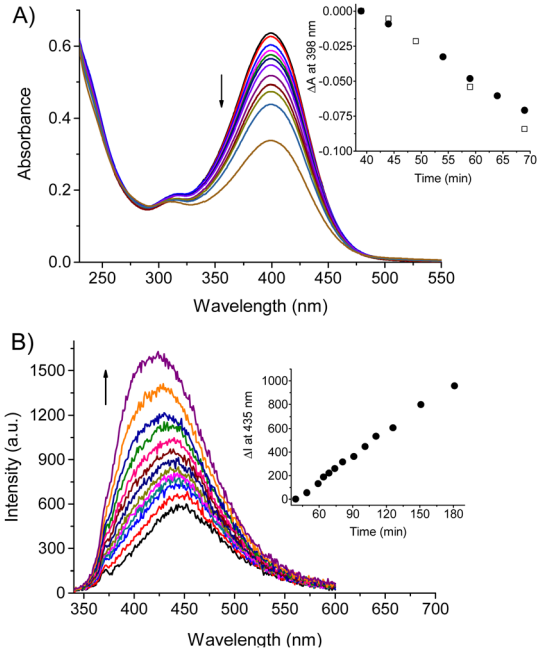

Fig. 6 (A) Absorption spectral changes observed upon exposure of an air-equilibrated aqueous solution (1% MeOH) of **NCDs-1** (26 μg mL^{-1}) previously irradiated for 39 min and then further irradiated at λ_{exc} = 405 nm at different irradiation times from 39 min to 180 min. The arrow indicates the course of the spectral profile with the illumination time. The inset shows the difference of absorbances observed at 398 nm for **NCDs-1** (●) and, for comparison, the free **1** (□), in the early stage of the photoreactions. (B) Fluorescence emission spectra related to the sample as in (A) recorded at λ_{exc} = 330 nm from 39 to 180 min. The inset shows the difference in the fluorescence intensity as a function of the irradiation time.

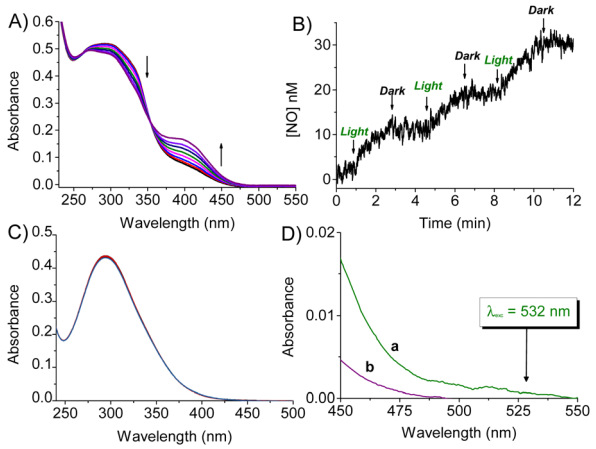

Fig. 7 (A) Absorption spectral changes observed upon exposure of an air-equilibrated aqueous solution (1% MeOH) of **NCDs-1** (26 μg mL^{-1}) at λ_{exc} = 532 nm at different irradiation times from 0 to 180 min. The arrows indicate the course of the spectral profile with the illumination time. (B) NO release profile observed for an air-equilibrated aqueous solutions (1% MeOH) of **NCDs-1** (26 μg mL^{-1}) upon alternate cycles of light irradiation at λ_{exc} = 532 nm. T = 25 °C. (C) Absorption spectral changes observed upon exposure of an air-equilibrated aqueous solution (1% MeOH) of **1** (16 μg mL^{-1}) at λ_{exc} = 532 nm at different irradiation times from 0 to 180 min. (D) Magnified view of the absorption spectra of aqueous solutions (1% MeOH) of **NCDs-1** (26 μg mL^{-1}) (a) and **1** (16 μg mL^{-1}) (b) in the spectral region 450–550 nm.

step is over, and the continuous emission increase of the second photolytic step (inset Fig. 6B) provides a readable indication of the total amount of NO being photogenerated.

The last remarkable point of **NCDs-1** is its capability to release NO even under the lower energy green light. Fig. 7A shows that irradiation of **NCDs-1** with 532 nm light leads to a photolysis profile identical to that observed upon irradiation with blue light (see Fig. 4A for comparison). In parallel, NO photorelease associated with this photolytic step was unambiguously demonstrated by its direct detection (Fig. 7B). On the other hand, no phototransformation of **1** was observed under otherwise identical experimental conditions (Fig. 7C). We believe that also in this case, the charge transfer band of **NCDs-1** has a role in triggering the NO photorelease. As shown in Fig. 7D, although very low, the absorption of this band is present at the excitation wavelength, in contrast to **1** alone.

Conclusions

We have prepared a nanoconjugate of **NCDs** and NOPDs gaining insights into its multifunctional properties which further validates the versatility of CD-based nanoplatforms as intriguing building blocks for the fabrication of fluorescent point sources of NO and heat addressed to bio-oriented studies.

The nanoconjugate **NCDs-1** exhibits a new absorption band which is not present in the simple physical mixture of the two components and attributable to a strong electronic interaction between them in the ground state. This new absorption is responsible for an enhancement of the NO photogeneration efficiency under blue light excitation by almost one order of magnitude with respect to the free NOPD and for the activation of photothermal conversion, which is negligible in the naked **NCDs**. The new absorption band in **NCDs-1** extends up to *ca.* 550 nm and, despite its low intensity, permits NO to be generated even upon excitation with the lower energy green light. The typical blue fluorescence of the naked **NCDs** is quenched in **NCDs-1**, initially due to the intramolecular charge transfer and after the NO detachment, due to a FRET mechanism. The sequential release of the second molecule of NO from the shell of the **NCDs** is accompanied by the suppression of the FRET process, leading to a restoration of the emission from the **NCD** core which acts as a useful optical NO reporter.

Experimental section

Materials and methods

NOPD **1** was prepared according to our previously reported procedure.[58] Naked **NCDs** were prepared according with the known hydrothermal synthetic protocol based on citric acid and urea as starting materials.[65] Briefly, 1.0 g of citric acid and 1.0 g of urea were dissolved in 25 mL water. The mixture was moved into a 50 mL Teflon autoclave and heated at 190 °C for 6 hours. Thereafter, the solution was cooled down to room

temperature to obtain a black/dark brown-coloured crude. The obtained product was centrifuged at 7000 rpm for 20 minutes to remove the larger sized particles. The brown-coloured supernatant was further dialyzed in water overnight by employing a dialysis membrane (1000 Da) in order to remove the unreacted reactants. Finally, the resultant solution was freeze-dried to obtain a black powder.

NCDs-1 were prepared as follows: 10 mg of **NCDs** were dispersed in 2 mL aqueous solution containing EDC (0.094 g, 0.49 mmol) and *N*-hydroxysuccinimide (NHS) (0.057 g, 0.029 mmol). The mixed solution was sonicated with the addition of the ice for 15 min in the dark. Then, 1 mL acetonitrile solution of **1** (20 mg) was added and stirred for 48 hours in the dark at room temperature. The solution was dialyzed to remove the residual starting materials, and then the solvent was freeze-dried to obtain the final product.

Fluorescence quantum yields (Φ_f) were determined at λ_{exc} = 330 nm using optically matched solutions at the excitation wavelength of **NCDs** or **NCDs-1** and anthracene as a standard through the eqn (1):

$$\Phi_f = \frac{\Phi_{f(s)} I_A n^2}{I_{A(s)} n_{(s)}{}^2} \quad (1)$$

where $\Phi_{f(s)}$ is the fluorescence quantum yield of the standard in ethanol ($\Phi_{f(s)}$ = 0.27);[75] I_A and $I_{A(s)}$ are the areas of the fluorescence spectra of **NCDs** or **NCDs-1**, and the standard, respectively; n and $n_{(s)}$ are the refraction index of the solvents used for **NCDs** or **NCDs-1**, and the standard. Absorbance at the excitation wavelength was less than 0.1 in all cases.

Photodecomposition quantum yields for step 1 ($\Phi_{1\text{-NO}}$) and 2 ($\Phi_{2\text{-NO}}$) in the case of free **1** were determined at λ_{exc} = 405 nm within the 20% transformation by using eqn (2):

$$\Phi = \frac{[X]V}{I(1-10^{-A})t} \quad (2)$$

where, [X] is the concentration of phototransformed **1** or **2**, V is the volume of the irradiated sample, I the intensity of the excitation light source, A is the absorbance of the sample at the excitation wavelength and t is the irradiation time. The concentrations of the phototransformed **1** and **2** were determined spectrophotometrically, by taking into account the absorption changes at 290 nm and 400 nm, and $\Delta\varepsilon_{290}$ = 8500 M^{-1} cm^{-1} and $\Delta\varepsilon_{400}$ = 9600 M^{-1} cm^{-1}, respectively. I was calculated by potassium ferrioxalate actinometry.

Photodecomposition quantum yields for step 1 ($\Phi_{1\text{-NO}}$) in the case of **NCDs-1** was calculated using the same equation as above but with X being the amount of NO photoreleased calculated by the amperogram.

The photothermal conversion efficiency η was calculated according to the literature,[76,77] using the following eqn (3):

$$\eta = \frac{hS(T_{max} - T_{surr}) - Q_{dis}}{I(1-10^{-A})} \quad (3)$$

where h represents the heat transfer coefficient, and S denotes the surface area of the container. The product hS is determined using eqn (6) and Fig. 5B. T_{max} is the equilibrium temperature and T_{surr} is the temperature of the surroundings (39 °C and 25.7 °C, respectively, from Fig. 5A). Q_{Dis} represents the heat dissipated from the light absorbed by the solvent and the container. I is the incident laser power applied and A is absorbance of the **NCDs-1** at the excitation wavelength.

To obtain hS, the dimensionless parameter θ is introduced as follows:

$$\theta = \frac{T - T_{surr}}{T_{max} - T_{surr}} \quad (4)$$

A sample system time constant τ_s can be determined as eqn (5).

$$t = -\tau_s \ln(\theta) \quad (5)$$

Based on Fig. 5B, τ_s was estimated and found to be 107.70 s.

$$hS = \frac{m_D C_D}{\tau_s} \quad (6)$$

The mass m_D is 0.1 g and the specific heat capacity C_D is 4.2 J g^{-1}·°C^{-1}. Therefore, using eqn (6), hS was calculated to be 3.90 mW °C^{-1}. Q_{dis} represents the heat dissipated from the light absorbed by the NMR tube and the solvent, and it was independently measured to be 32.34 mW using the borosilicate glass NMR tube filled with pure water with 1% MeOH.

Instrumentation

UV-vis spectra absorption and fluorescence emission spectra were recorded with a PerkinElmer spectrophotometer (mod. Lambda 365) and a Spex Fluorolog-2 (mod. F-111) spectrofluorimeter, respectively, using either quartz cells with a path length of 1 cm. FTIR spectra were recorded with a System 2000 (PerkinElmer, Waltham, MA, USA).

HR-TEM images were taken with a scanning transmission electron microscope (S/TEM), JEOL JEM F200, at the maximum electron voltage of 200 kV. TEM grids were prepared by drop-casting of an aqueous dispersion of the samples onto 400 mesh carbon-coated Cu grids, followed by air-drying.

Photothermal experiments were performed by irradiating the samples (100 μL) in an NMR tube with a 405 nm continuous-wave (CW) laser (*ca.* 250 mW cm^{-2}) having a beam diameter of *ca.* 1.5 mm and detecting the temperature changes with a FLIR C3 thermal imaging camera. Pictures are edited using FLIR tools software and presented with a linear colour scale for temperature.

Steady-state irradiation photolysis experiments were performed in a thermostatted quartz cell (1 cm pathlength, 3 mL capacity) under gentle stirring using CW laser sources at λ_{exc} = 405 nm or 532 nm.

Direct monitoring of NO release for samples in solution was performed by amperometric detection with a World Precision Instrument, ISO-NO meter, equipped with a data acquisition system, and based on direct amperometric detection of NO with short response time (<5 s) and sensitivity range 1 nM–20 μM. The analog signal was digitalized using a four-channel recording system and transferred to a PC. The sensor was accurately calibrated by mixing standard solutions of $NaNO_2$ with 0.1 M H_2SO_4 and 0.1 M KI according to the reaction:

$$4H^+ + 2I^- + 2NO_2^- \rightarrow 2H_2O + 2NO + I_2$$

Irradiation was performed in a thermostatted quartz cell (1 cm pathlength, 3 mL capacity) using the above CW laser at λ_{exc} = 405 nm or 532 nm. NO measurements were carried out under stirring with the electrode positioned outside the light path to avoid NO signal artifacts due to photoelectric interference on the ISO-NO electrode.

Data availability

Data for this article, including [Fig. 1–7] are available at [Zenodo] at [**https://Zenodo.org**].

Conflicts of interest

We have no conflict of interest to declare.

Acknowledgements

This research was funded by the European Union – NextGenerationEU through the Italian Ministry of University and Research under PNRR – M4C2-I1.3 Project PE_00000019 ''HEAL ITALIA'' and PNRR-M4C2-I1.1 – MUR Call for proposals n. by PNRR-M4C2-I1.1 – 1409 of 14-09-2022 – PRIN 2022 PNRR – ERC sector PE4 – Project title: A molecular platform for intracellular nitric oxide sensing – Project Code P2022F4WR8-CUP Code D53D23016840001.

Notes and references

1 L. Đorđević, F. Arcudi, M. Cacioppo and M. Prato, *Nat. Nanotechnol.*, 2022, **17**, 112–130.
2 N. V. Tepliakov, E. V. Kundelev, P. D. Khavlyuk, Y. Xiong, M. Yu Leonov, W. Zhu, A. V. Baranov, A. V. Fedorov, A. L. Rogach and I. D. Rukhlenko, *ACS Nano*, 2019, **13**, 10737–10744.
3 S. Zhu, Y. Song, J. Shao, X. Zhao and B. Yang, *Angew. Chem., Int. Ed.*, 2015, **54**, 14626–14637.
4 C. J. Reckmeier, J. Schneider, A. S. Susha and A. L. Rogach, *Opt. Express*, 2016, **24**, A312–A340.
5 W. Liu, C. Li, Y. Ren, X. Sun, W. Pan, Y. Li, J. Wang and W. Wang, *J. Mater. Chem. B*, 2016, **4**, 5772–5788.
6 M. Bruchez, M. Moronne, P. Gin, S. Weiss and A. P. Alivisatos, *Science*, 1998, **281**, 2013–2016.
7 J. Peng, W. Gao, B. K. Gupta, Z. Liu, R. Romero-Aburto, L. Ge, L. Song, L. B. Alemany, X. Zhan, G. Gao, S. A. Vithayathil, B. A. Kaipparettu, A. A. Marti, T. Hayashi, J.-J. Zhu and P. M. Ajayan, *Nano Lett.*, 2012, **12**, 844–849.
8 Y. Li, Y. Hu, Y. Zhao, G. Shi, L. Deng, Y. Hou and L. Qu, *Adv. Mater.*, 2011, **6**, 776–780.
9 L. Cao, S. Sahu, P. Anilkumar, C. E. Bunker, J. Xu, K. A. S. Fernando, P. Wang, E. A. Guliants, K. N. I. Tackett and Y.-P. Sun, *J. Am. Chem. Soc.*, 2011, **133**, 4754–4757.
10 G. J. Kavarnos, *Photoinduced Electron Transfer I*, Springer Berlin Heidelberg, 1990.
11 I. Srivastava, J. S. Khamo, S. Pandit, P. Fathi, X. Huang, A. Cao, R. T. Haasch, S. Nie, K. Zhang and D. Pan, *Adv. Funct. Mater.*, 2019, **29**, 1902466.
12 A. Cadranel, J. T. Margraf, V. Strauss, T. Clark and D. M. Guldi, *Acc. Chem. Res.*, 2019, **52**, 955–963.
13 C. Hu, M. Li, J. Qiu and Y.-P. Sun, *Chem. Soc. Rev.*, 2019, **48**, 2315–2337.
14 C. X. Guo, H. B. Yang, Z. M. Sheng, Z. S. Lu, Q. L. Song and C. M. Li, *Angew. Chem., Int. Ed.*, 2010, **49**, 3014–3017.
15 K. A. S. Fernando, S. Sahu, Y. Liu, W. K. Lewis, E. A. Guliants, A. Jafariyan, P. Wang, C. E. Bunker and Y.-P. Sun, *ACS Appl. Mater. Interfaces*, 2015, **7**, 8363–8376.
16 M. Sbacchi, M. Mamone, L. Morbiato, P. Gobbo, G. Filippini and M. Prato, *ChemCatChem*, 2023, **15**, e202300667.
17 F. Yuan, S. Li, Z. Fan, X. Meng, L. Fan and S. Yang, *Nano Today*, 2016, **11**, 565–586.
18 X. Zhang, Y. Zhang, Y. Wang, S. Kalytchuk, S. V. Kershaw, Y. Wang, P. Wang, T. Zhang, Y. Zhao, H. Zhang, T. Cui, Y. Wang, J. Zhao, W. W. Yu and A. L. Rogach, *ACS Nano*, 2013, **7**, 11234–11241.
19 L. Đorđević, F. Arcudi, A. D'Urso, M. Cacioppo, N. Micali, T. Bürgi, R. Purrello and M. Prato, *Nat. Commun.*, 2018, **9**, 3442.
20 D. Li, P. Jing, L. Sun, Y. An, X. Shan, X. Lu, D. Zhou, D. Han, D. Shen, Y. Zhai, S. Qu, R. Zbořil and A. L. Rogach, *Adv. Mater.*, 2018, **30**, 1705913.
21 M. Behi, L. Gholami, S. Naficy, S. Palomba and F. Dehghani, *Nanoscale Adv.*, 2022, **4**, 353–376.
22 J. Tang, B. Kong, H. Wu, M. Xu, Y. Wang, Y. Wang, D. Zhao and G. Zheng, *Adv. Mater.*, 2013, **25**, 6569–6574.
23 J. Zhang, X. Lu, D. Tang, S. Wu, X. Hou, J. Liu and P. Wu, *ACS Appl. Mater. Interfaces*, 2018, **10**, 40808–40814.
24 T. Zhang, J. Wu, Z. Tang and S. Qu, *Mater. Chem. Front.*, 2023, **7**, 2359–2372.
25 L. Cao, X. Wang, M. J. Meziani, F. Lu, H. Wang, P. G. Luo, Y. Lin, B. A. Harruff, L. M. Veca, D. Murray, S.-Y. Xie and Y.-P. Sun, *J. Am. Chem. Soc.*, 2007, **129**, 11318–11319.
26 K. O. Boakye-Yiadom, S. Kesse, Y. Opoku-Damoah, M. S. Filli, M. Aquib, M. M. B. Joelle, M. A. Farooq, R. Mavlyanova, F. Raza, R. Bavi and B. Wang, *Int. J. Pharm.*, 2019, **564**, 308–317.
27 B. Li, S. Zhao, L. Huang, Q. Wang, J. Xiao and M. Lan, *J. Chem. Eng.*, 2021, **408**, 127245.
28 L. J. Ignarro, *Arch. Pharm. Res.*, 2009, **32**, 1099–1101.
29 L. J. Ignarro, *Nitric Oxide: Biology and Pathobiology*, Elsevier Inc., 2nd edn, 2010.
30 G. Walford and J. Loscalzo, *JTH*, 2003, **1**, 2112–2118.
31 F. C. Fang, *Nitric Oxide and Infection*, Springer, US, 2002.
32 C. Bogdan, *Nat. Immunol.*, 2001, **2**, 907–916.
33 D. A. Wink, K. M. Miranda, M. G. Espey, R. M. Pluta, S. J. Hewett, C. Colton, M. Vitek, M. Feelisch and M. B. Grisham, *ARS*, 2001, **3**, 203–213.
34 J. Luo and A. F. Chen, *Acta Pharmacol. Sin.*, 2005, **26**, 259–264.
35 B. Bonavida, S. Khineche, S. Huerta-Yepez and H. Garbán, *Drug Resist. Updates*, 2006, **9**, 157–173.

36 C. Farah, L. Y. M. Michel and J. L. Balligand, *Nat. Rev. Cardiol.*, 2018, **15**, 292–316.
37 P. Vallance, *Fundam. Clin. Pharmacol.*, 2003, **17**, 1–10.
38 Z. Huang, J. Fu and Y. Zhang, *J. Med. Chem.*, 2017, **60**, 7617–7635.
39 A. W. Carpenter and M. H. Schoenfisch, *Chem. Soc. Rev.*, 2012, **41**, 3742–3752.
40 D. A. Wink and J. B. Mitchell, *Free Radical Biol. Med.*, 1998, **25**, 434–456.
41 S. Sortino, *Chem. Soc. Rev.*, 2010, **39**, 2903–2913.
42 P. C. Ford, *Coord. Chem. Rev.*, 2018, **376**, 548–564.
43 N. L. Fry and P. K. Mascharak, *Acc. Chem. Res.*, 2011, **44**, 289–298.
44 N. Ieda, Y. Oka, T. Yoshihara, S. Tobita, T. Sasamori, M. Kawaguchi and H. Nakagawa, *Sci. Rep.*, 2019, **9**, 1430.
45 S. Sortino, *J. Mater. Chem.*, 2012, **22**, 301–318.
46 D. Afonso, S. Valetti, A. Fraix, C. Bascetta, S. Petralia, S. Conoci, A. Feiler and S. Sortino, *Nanoscale*, 2017, **9**, 13404–13408.
47 C. Fowley, A. P. McHale, B. McCaughan, A. Fraix, S. Sortino and J. F. Callan, *Chem. Commun.*, 2015, **51**, 81–84.
48 Q. Deng, H.-J. Xiang, W.-W. Tang, L. An, S.-P. Yang, Q.-L. Zhang and J.-G. Liu, *J. Inorg. Biochem.*, 2016, **165**, 152–158.
49 M. Guo, H.-J. Xiang, Y. Wang, Q.-L. Zhang, L. An, S.-H. Ping Yang, Y. Ma, Y. Wang and J.-G. Liu, *Chem. Commun.*, 2017, **53**, 3253–3256.
50 A. Fraix, C. Parisi, M. Seggio and S. Sortino, *Chem. – Eur. J.*, 2021, **27**, 12714–12725.
51 A. Fraix, N. Marino and S. Sortino, *Top. Curr. Chem.*, 2016, **370**, 225–257.
52 C. Parisi, A. Pastore, M. Stornaiuolo and S. Sortino, *J. Mater. Chem. B*, 2024, **12**, 5076–5084.
53 T. J. Martins, C. Parisi, J. Guerra Pinto, I. de Paula Ribeiro Brambilla, M. Malanga, J. Ferreira-Strixino and S. Sortino, *ACS Med. Chem. Lett.*, 2024, **15**, 857–863.
54 N. Ieda, Y. Hotta, N. Miyata, K. Kimura and H. Nakagawa, *J. Am. Chem. Soc.*, 2014, **136**, 7085–7091.
55 E. Y. Zhou, H. Knox, C. J. Reinhardt, G. Partipilo, M. J. Nilges and J. Chan, *J. Am. Chem. Soc.*, 2018, **140**, 11686–11697.
56 C. Parisi, M. Seggio, A. Fraix and S. Sortino, *ChemPhotoChem*, 2020, **4**, 742–748.
57 C. Parisi, M. Failla, A. Fraix, L. Menilli, F. Moret, E. Reddi, B. Rolando, F. Spyrakis, L. Lazzarato, R. Fruttero, A. Gasco and S. Sortino, *Chem. Sci.*, 2021, **12**, 4740–4746.
58 C. Parisi, M. Failla, A. Fraix, B. Rolando, E. Gianquinto, F. Spyrakis, E. Gazzano, C. Riganti, L. Lazzarato, R. Fruttero, A. Gasco and S. Sortino, *Chem. – Eur. J.*, 2019, **25**, 11080–11084.
59 A. Fraix, C. Parisi, M. Failla, K. Chegaev, F. Spyrakis, L. Lazzarato, R. Fruttero, A. Gasco and S. Sortino, *Chem. Commun.*, 2020, **56**, 6332–6335.
60 C. Parisi, A. Fraix, S. Guglielmo, F. Spyrakis, B. Rolando, L. Lazzarato, R. Fruttero, A. Gasco and S. Sortino, *Chem. – Eur. J.*, 2020, **26**, 13627–13633.
61 F. Laneri, M. Seggio, C. Parisi, S. Béni, A. Fraix, M. Malanga and S. Sortino, *ACS Appl. Polym. Mater.*, 2023, **5**, 7918–7926.
62 A. Fraix, V. Kirejev, M. Malanga, E. Fenivesi, S. Beni, M. B. Ericson and S. Sortino, *Chem. – Eur. J.*, 2019, **23**, 7091–7095.
63 M. Malanga, M. Seggio, V. Kirejev, A. Fraix, I. Di Bari, E. Fenyvesi, M. B. Ericson and S. Sortino, *Biomater. Sci.*, 2019, **7**, 2272–2276.
64 E. B. Caruso, S. Petralia, S. Conoci, S. Giuffrida and S. Sortino, *J. Am. Chem. Soc.*, 2007, **129**(3), 480–481.
65 H. Qi, L. Qiu, X. Zhang, T. Yi, J. Jing, R. Sami, S. F. Alanazi, Z. Alqahtani, M. D. Aljabri and M. M. Rahmani, *RSC Adv.*, 2023, **13**, 2663–2671.
66 H. Nie, M. Li, Q. Li, S. Liang, Y. Tan, L. Sheng, W. Shi and S. Xiao-An Zhang, *Chem. Mater.*, 2014, **26**, 3104–3112.
67 A. Ferrer-Ruiz, T. Scharl, L. Rodríguez-Pérez, A. Cadranel, M. Á. Herranz, N. Martín and D. M. Guldi, *J. Am. Chem. Soc.*, 2020, **142**, 20324–20328.
68 X.-Q. Zhu, J.-Q. He, Q. Li, M. Xian, J. Lu and J.-P. Cheng, *J. Org. Chem.*, 2000, **65**, 6729–6735.
69 A. Fraix, C. Parisi, G. Longobardi, C. Conte, A. Pastore, M. Stornaiuolo, A. C. E. Graziano, M. E. Alberto, A. Francés-Monerris, F. Quaglia and S. Sortino, *Biomacromolecules*, 2023, **24**, 3887–3897.
70 F. Laneri, C. Parisi, M. Seggio, A. Fraix, G. Longobardi, O. Catanzano, F. Quaglia and S. Sortino, *J. Mater. Chem. B*, 2024, **12**, 6500–6508.
71 A. R. Gopal, F. Joy, V. Dutta, J. Devasia, R. Dateer and A. Nizam, *Part. Part. Syst. Charact.*, 2024, **41**, 2300072.
72 P. C. Ray, Z. Fan, R. A. Crouch, S. S. Sinha and A. Pramanik, *Chem. Soc. Rev.*, 2014, **43**, 6370.
73 S. Miao, K. Liang and B. Kong, *Mater. Chem. Front.*, 2020, **4**, 128.
74 C. Wei, X. Jin, C. Wu, A. Brozovic and W. Zhangm, *Diamond Relat. Mater.*, 2022, **126**, 109048.
75 M. Montalti, A. Credi, L. Prodi and M. T. Gandolfi, *Handbook of Photochemistry*, CRC, Boca Raton, 3rd edn, 2006.
76 X. Liu, B. Li, F. Fu, K. Xu, R. Zou, Q. Wang, B. Zhang, Z. Chen and J. Hu, *Dalton Trans.*, 2014, **43**, 11709–11715.
77 X. Cui, Q. Ruan, X. Zhuo, X. Xia, J. Hu, R. Fu, Y. Li, J. Wang and H. Xu, *Chem. Rev.*, 2023, **123**, 6891–6952.